Neovascularization, Enhanced Inflammatory Response, and Age-Related Cone Dystrophy in the *Nrl*$^{-/-}$*Grk1*$^{-/-}$ Mouse Retina

Rosanne M. Yetemian,[1] *Bruce M. Brown,*[1] *and Cheryl M. Craft*[1,2]

Purpose. The effects of aging and light exposure on cone photoreceptor survival were compared between mouse retinas of neural retina leucine zipper knockout (*Nrl*$^{-/-}$) mice and double-knockout mice lacking G-protein–coupled receptor kinase 1 (*Nrl*$^{-/-}$*Grk1*$^{-/-}$).

Methods. Mice were reared in total darkness, ambient cyclic light, or constant light, and their retinas were evaluated from 1 to 9 months of age using immunohistochemistry, electroretinography, and fluorescein angiography. Retinal gene expression and statistically significant probe sets were categorized using analysis software. Select gene expression changes were confirmed with quantitative RT-PCR.

Results. In contrast to retinas from *Nrl*$^{-/-}$, those from *Nrl*$^{-/-}$*Grk1*$^{-/-}$ exhibit a progressive loss of the outer nuclear layer, retinal physiology deficits, and a higher rate of degeneration with increasing age that is independent of environmental light exposure. Changes in retinal neovascularization occur in the *Nrl*$^{-/-}$*Grk1*$^{-/-}$ at 1 month, before the onset of significant cone functional deficits. Microarray analyses demonstrate statistically significant changes in transcript levels of more than 400 genes, of which the oncostatin M signaling pathway and the inflammatory disease response network were identified.

Conclusions. These data demonstrate that the loss of functional Grk1 on the enhanced S-cone *Nrl*$^{-/-}$ background exacerbates age-related cone dystrophy in a light-independent manner, mediated partly through the inflammatory response pathway and neovascularization. According to these findings, Grk1 helps to maintain a healthy cone environment, and the *Nrl*$^{-/-}$*Grk1*$^{-/-}$ mouse allows examination of the alternative roles of Grk1 in cone photoreceptor homeostasis. (*Invest Ophthalmol Vis Sci.* 2010;51:6196–6206) DOI:10.1167/iovs.10-5452

From the [1]Mary D. Allen Laboratory for Vision Research, Doheny Eye Institute, Department of Ophthalmology, Division of Retinal Molecular Biology, and the [2]Department of Cell and Neurobiology, Keck School of Medicine, University of Southern California, Los Angeles, California.

Supported by National Institutes of Health Grant EY015851 (CMC); National Eye Institute Core Grant EY03040 (Doheny Eye Institute); Research to Prevent Blindness (Doheny Eye Institute); Foundation Fighting Blindness (Doheny Eye Institute); William Hansen Sandberg Memorial Foundation (RMY, CMC); FARVO Richard Newton Lolley Travel Award (RMY); Thomas and Laurie Gray; Tony Gray Foundation; Dorie Miller; Patricia Beckman; and the Mary D. Allen Foundation (CMC).

Submitted for publication February 27, 2010; revised June 21, 2010; accepted July 21, 2010.

Disclosure: **R.M. Yetemian**, None; **B.M. Brown**, None; **C.M. Craft**, None

Corresponding author: Cheryl M. Craft, Mary D. Allen Laboratory for Vision Research, Doheny Eye Institute, Department of Ophthalmology, Division of Retinal Molecular Biology, Keck School of Medicine, University of Southern California, 1355 San Pablo Street, DVRC 405, Los Angeles, CA 90033-9224; ccraft@usc.edu.

Significant advances in bioinformatics have identified essential genetic links and characterized basic molecular mechanisms driving the components of the visual G-protein–coupled receptor (GPCR) signal transduction cascade leading to rod photoreceptor cell death. However, with a population of 3% to 5% cone photoreceptors in the mouse retina, the manifestations of GPCR cascade disruption on cones have only recently been studied with the help of the neural retina leucine zipper knockout (*Nrl*$^{-/-}$) mouse model.[1] In humans, a loss-of-function mutation in the *NRL* gene leads to an autosomal recessive disorder, enhanced S-cone syndrome, which causes an excess number of S cones. Symptoms include night blindness, variable loss of visual acuity, and visual field abnormalities.[2]

Because of a developmental cell switch from rod to short-wavelength (SWL) pigment photoreceptors, the Nrl transcription factor provides a unique opportunity with which to study cone phototransduction mechanisms given that rod phototransduction components, including rhodopsin, are absent. Photopic electrophysiological analyses of *Nrl*$^{-/-}$ retinas reveal that the amplitude of light-adapted electroretinographic (ERG) responses elicited by maximum stimulus are stable up to 31 weeks of age, suggesting cones survive without rod function.[1] Extensive ultrastructural, biochemical, and electrophysiological characterization of the *Nrl*$^{-/-}$ mouse photoreceptors demonstrate that the photoreceptors have many of the phenotypic hallmarks of cones.[1,3,4] Results from gene expression profiling of the *Nrl*$^{-/-}$ mouse retina with microarray technology (GeneChip; Affymetrix, Santa Clara, CA) further support the concept that the rod precursors in the *Nrl*$^{-/-}$ retina differentiate as cones instead of rods and therefore exhibit an enhanced S-cone population, with the caveat that they are mutant cones and different from those found in a wild-type (WT) retina.[2]

Another essential regulatory component in the phototransduction cascade is the serine/threonine G-protein–coupled receptor kinase 1 (Grk1; rhodopsin kinase), which is expressed in both rods and cones in rod-dominant human, monkey, and mouse[5–8] and in cone-dominant chicken.[9] Grk1 phosphorylation of light-activated rhodopsin is required for normal phototransduction inactivation in vivo.[10,11] Although the cone-specific Grk7 is expressed in various species,[6,11–13] only Grk1 is expressed in the mouse photoreceptor. With the creation of a double-knockout mouse lacking both Grk1 and Nrl, the electrophysiological analyses of mouse cone photoresponses clearly demonstrated that Grk1 plays a critical role in the phosphorylation of S and M opsins and in the inactivation and normal recovery of cone pigments.[3,5,8]

The *Nrl*$^{-/-}$*Grk1*$^{-/-}$ mouse provides an invaluable model not only for the study of cone GPCR signaling pathways but also for the molecular balance between cone photoreceptor survival and death in inherited retinal diseases. Unlike the rod photoreceptors

of the *Grk1*$^{-/-}$ mouse, which degenerate rapidly when exposed to light because of the inability to inactivate phototransduction,[14] cones lacking Grk1 expression on the *Nrl*$^{-/-}$ background degenerate by apoptosis in the dark.[15] The present study extends our initial observations and demonstrates that in addition to a delayed photoresponse recovery, the absence of Grk1 expression leads to age-related and light-independent cone dystrophy with abnormal vascularization in the retinas of *Nrl*$^{-/-}$*Grk1*$^{-/-}$ mice compared with *Nrl*$^{-/-}$. To facilitate the identification of potential genes involved in biological and disease pathways, we identified key molecular networks to characterize the *Nrl*$^{-/-}$*Grk1*$^{-/-}$ phenotype. Taken together, these data allow us to hypothesize that, aside from its known function in photoreceptor pigment recovery, Grk1 plays a functional role in the homeostasis of a healthy cone environment.

METHODS

Experimental Animals

All mice were treated according to the guidelines established by the Institute for Laboratory Animal Research and the ARVO Statement for the Use of Animals in Ophthalmic and Vision Research. The Institutional Animal Care and Use Committee of the University of Southern California approved all procedures involved in animal experiments. Control mice used for all experiments were C57/Bl6J (C57) mice that were born and maintained in 12-hour light/12-hour dark cycles.

Knockout mice *Nrl*$^{-/-}$ (provided by Anand Swaroop[1]) and *Grk1*$^{-/-}$ (provided by C.-K. Jason Chen[14]) were created from a mixture of C57/Bl6J and 129/SvJ founders and are, therefore, on a similar mixed genetic background. The *Nrl*$^{-/-}$*Grk1*$^{-/-}$ mice were created by backcrossing *Nrl*$^{-/-}$ mice with *Grk1*$^{-/-}$ mice, as described previously.[8] The *Nrl*$^{-/-}$ and *Nrl*$^{-/-}$*Grk1*$^{-/-}$ mice were born and maintained in total darkness, ambient light (5 lux white light measured at the cage level), 12-hour light/12-hour dark cycles, or constant bright light (approximately 8000 lux white light measured at the cage level).

Electroretinography

Electroretinograms were recorded as previously described.[15–17] The *Nrl*$^{-/-}$ and *Nrl*$^{-/-}$*Grk1*$^{-/-}$ mice maintained in total darkness, ambient (~5 lux) cyclic light, or bright (~8000 lux) constant light were recorded at 1, 3, 5, 7, and 9 months of age. At least 10 mice were recorded for each genotype at each age. The *Nrl*$^{-/-}$ and *Nrl*$^{-/-}$*Grk1*$^{-/-}$ mice were dark adapted overnight, and their eyes were dilated with topical administration of phenylephrine (2.5%) and tropicamide (0.5%). Mice were anesthetized by intraperitoneal injection of ketamine hydrochloride (100 mg/kg body weight) and xylazine hydrochloride (10 mg/kg body weight), and their corneas were anesthetized with 0.5% tropical tetracaine. Each mouse was placed in an aluminum foil-lined Faraday cage, and a DLT fiber electrode was placed on the right cornea. A platinum reference electrode was placed on the lower eyelid, and another ground electrode was placed on the ipsilateral ear. Photopic stimuli of 10-μs duration of a maximum light intensity (log 2.01 cd $\cdot$ s/m^2) were delivered through one arm of a coaxial cable using a xenon flash (PS22; Grass Instruments, West Warwick, RI). The cable delivered the flash 5 mm from the surface of the cornea, and a background light (200 cd/m^2) with spectral peaks at 485, 530, and 543 nm and minimal transmission below 400 nm was used. Dark-adapted maximum responses were measured using the nonattenuated light stimulus. The b-wave amplitude was measured from the trough of the a-wave to the peak of the b-wave.

Eyecup Preparation

All mice were euthanized by overdose of carbon dioxide inhalation either at midday under fluorescent lights or in total darkness. Retinas were dissected either under room light using a dissecting scope or in total darkness with infrared goggles and an infrared-equipped dissecting microscope. Eyes from each genotype and age examined were enucleated, marked for orientation (if dissected in the light), and fixed with 4% paraformaldehyde in phosphate-buffered saline (PBS) for at least 2 hours. Each eyecup was washed twice in PBS for 5 minutes, then dehydrated in a solution of 30% (wt/vol) sucrose in PBS overnight at 4°C. Each eyecup was then embedded in OCT media (Sakura Finetek, Torrance, CA)[18] and frozen in liquid nitrogen. Retinal cryosections at 8-μm thickness were cut along the vertical meridian through the optic nerve and were placed on poly (L-lycine)– coated glass slides.

Retinal Histology

To examine the morphologic changes associated with a decrease in b-wave amplitude in *Nrl*$^{-/-}$*Grk1*$^{-/-}$ mice compared with *Nrl*$^{-/-}$ controls, six mice of both genotypes at 1, 5, and 9 months of age were used. Because the decrease in cone function by ERG analysis is light independent, retinal sections used in hematoxylin and eosin (H&E) studies were from mice born and maintained in ambient cyclic light.

Briefly, retinal sections were pre-rinsed in double-distilled water (ddH_2O), then dipped in Harris hematoxylin for 45 seconds followed by a wash in ddH_2O. Slides were subsequently dipped in acid alcohol (70% ethanol, 1% HCl) for 1 minute, washed in ddH_2O, dipped five times in ammonia water (0.3% NH_4OH), and washed. Slides were then dipped in eosin-phloxine for 1 minute, then dehydrated in a series of 95% ethanol and 100% ethanol followed by 6 minutes in xylene. Once the slides were dried, mounting medium was applied and slides were coverslipped.

Immunohistochemistry

Immunohistochemistry (IHC) is a well-established technique for the identification and localization of proteins expressed within the mouse retina. For all IHC experiments, our established protocol was followed with minor modifications.[18] Frozen retinal sections of *Nrl*$^{-/-}$ and *Nrl*$^{-/-}$*Grk1*$^{-/-}$ mice were blocked in IHC blocking buffer (10% normal goat serum, 1% bovine serum albumin, 0.2% Triton X-100 in PBS) for 30 minutes, then incubated with the mouse anti-Arrestin4 (Arr4) rabbit polyclonal antibody (pAB mCAR-LUMIJ) or the mouse anti-S or anti-M opsin peptide rabbit polyclonal antibodies, as described previously.[8] All three antibodies were diluted to 1:1000 in PBS and were incubated for 1 hour at room temperature. Animals were similarly stained using the mouse anti-VEGF antibody (Abcam, Cambridge, UK) at a dilution of 1:200 in PBS incubated overnight at 4°C. After three 5-minute washes in PBS, the slides probed with pAB mCAR-LUMIJ and pAB S- or M-opsin were incubated in fluorescein anti–rabbit IgG (1:200; Vector Laboratories, Burlingame, CA) for 1 hour at room temperature. Slides were either mounted with mounting medium (Vectashield; Vector Laboratories) for fluorescence with DAPI (Vector Laboratories) or incubated with monomeric cyanine nucleic acid stain (To-Pro3 iodide; 1:2000; Invitrogen, Carlsbad, CA), mounted with mounting medium (Vectashield; Vector Laboratories), and coverslipped.

Slides prepared for IHC or H&E were photographed with a digital camera (SPOT model SP401–115, software version 3.5.0; Diagnostic Instruments, Inc., Sterling Heights, MI) mounted to a fluorescent microscope (DMR; Leica Microsystems, Wetzlar GmbH, Wetzlar, Germany).[17]

TUNEL Analysis of Apoptosis

Functional cone photoreceptor deficits in *Nrl*$^{-/-}$ and *Nrl*$^{-/-}$*Grk1*$^{-/-}$ mice were evident by 3 months; therefore, to verify cone apoptosis before outer nuclear layer (ONL) thinning, five 1-month-old mice from control C57/Bl6J, *Nrl*$^{-/-}$ and *Nrl*$^{-/-}$*Grk1*$^{-/-}$ genotypes each and three postnatal day (P) 21 mice from C57/Bl6J, *Nrl*$^{-/-}$ and *Nrl*$^{-/-}$*Grk1*$^{-/-}$ genotypes each were born and maintained in ambient cyclic light and euthanized in the light. Both eyes were fixed and embedded as described for retinal histology. Three adjacent sections cut through the optic nerve along the vertical meridian were used from each eye. Apoptotic cells were visualized by means of the terminal deoxynucleotidyl transferase-mediated dUTP nick-end labeling (TUNEL) assay using a fluorometric TUNEL system (DeadEnd; Promega, Madison, WI) according to the manufacturer's instructions.[19] After labeling, the slides were mounted with mounting medium (Vectashield; Vector Laboratories) for fluorescence with DAPI nuclear stain (Vector Laboratories).

Apoptotic cells were quantified by counting TUNEL-positive cells from the entire section, and the average number of apoptotic cells per section was calculated from three sections of all eyes from each genotype. Statistical analysis was performed using the one-way ANOVA with Bonferroni's correction for repeated measures.

Microarray and Ingenuity Pathway Analysis

Transcriptional variability when apoptosis was documented and before severe morphologic changes was examined in retinas from 1-month-old light-adapted *Nrl*$^{-/-}$ and *Nrl*$^{-/-}$*Grk1*$^{-/-}$ mice. Retinas were homogenized and total RNA isolated using a monophasic phenol and guanidine isothiocyanate solution extraction (TRIzol; Invitrogen) according to the manufacturer's instructions. Retinas at this age also have ONLs of similar thickness, which allowed for comparable mRNA levels between the two strains. RNA purity and concentration were determined using spectrophotometry A_{260}/A_{280} ratios. Microarray technology (Mouse Genome 430 2.0 GeneChips; Affymetrix, Inc.) was used for hybridization. RNA isolation and microarray hybridization were performed in triplicate for statistical and biological relevance. The original Affymetrix raw intensity files were imported into statistical analysis software (Genomic Suite; Partek, Inc., St. Louis, MO) and preprocessed using the software-implemented GCRMA background correction[20] and quantile normalization algorithms.[21] The $\log_2$-transformed data were then subjected to a two-way mixed-model factorial ANOVA, and the list of differentially expressed genes between the two genotypes was subsequently generated ($P < 0.005$ coupled with fold changes >1.2 or <-1.2). Transcripts with statistically significant differences and annotated function were categorized using ingenuity pathway analysis (IPA; Ingenuity Systems, Redwood City, CA). Statistical significance of canonical pathways was conducted using Fisher's exact test with a *P* value threshold of 0.05. Ratios are the number of molecules identified from the data set per pathway. Scores for top networks were based on the hypergeometric distribution and calculated with the right-tailed Fisher's exact test by IPA.

Real-Time Quantitative Polymerase Chain Reaction

To verify the microarray results for pituitary tumor transforming gene 1 (*Pttg1*) and kallikrein 2 (*Klk2*), retinas were collected for RNA isolation from light-adapted 1-month-old *Nrl*$^{-/-}$ and *Nrl*$^{-/-}$*Grk1*$^{-/-}$ mice using first-strand cDNA synthesis (Invitrogen). Briefly, 1 μg total RNA was reverse transcribed into first-strand cDNA using 200 U/μL reverse transcriptase (SuperScript III; Invitrogen), 40 U/μL RNase (OUT; Invitrogen), and 50 μM Oligo$(dT)_{20}$ random hexamer primers and was incubated at 50°C for 50 minutes. All cDNA synthesis reactions were treated with endonuclease (RNase H; Invitrogen) and stored at −20°C. Primers used for qPCR were as follows: +m*Pttg1,* CCCTTTCTATCATGGGAATCTG; −m*Pttg1,* GGCAATTCAACATCCAGAGTG; +m*Klk2,* GGCTGGGGCAGCATTAACCAGT; −m*Klk2,* TCATTAGGATGGAGCTTGATGGACAC; +mβ-actin, ATGGAATCCTGTGGCATCCA; −m-β-actin CGCTCAGGAGGAGCAATGAT.

Real-time q-PCR was performed by monitoring dye fluorescence (RT^2 SYBR Green; SABiosciences, Frederick, MD) using a thermal cycler platform with a fluorescence detection system and high-quality reagents (LightCycler Systems for Real-Time PCR; Roche Applied Science, Penzberg, Germany). The PCR reaction included 1 μL cDNA corresponding to 2 to 4 ng total RNA, SYBR Green, ddH_2O, and 10 μm PCR primer pairs. β-Actin was used as the reference gene. Cycling conditions were 95°C for 10 minutes, followed by 45 cycles of 95°C for 15 seconds and 60°C for 1 minute for quantification. The melting curve was calculated using 1 cycle of 95°C for 1 minute and 65°C for 2 minutes, followed by continuous acquisition at 97°C and cooling at 40°C. Melting curve analysis confirmed the absence of primer dimers.

Endothelial Cell Staining

To further characterize changes in retinal morphology, we used fluorescein-labeled GSL isolectin B_4 (Vector Laboratories) as a marker to selectively stain vascular cells. Retinas from P21 and 1-month-old and *Nrl*$^{-/-}$ and *Nrl*$^{-/-}$*Grk1*$^{-/-}$ mice raised in cycling light were dissected, fixed, and sectioned as described.[8,22] Sections were dried, then blocked with 1% bovine serum albumin in PBS for 30 minutes. In a humidified chamber, slides were incubated with isolectin B_4 (1:1000) for 1 hour at room temperature, washed in PBS, and mounted with mounting medium (Vectashield; Vector Laboratories) for fluorescence with DAPI (Vector Laboratories) and coverslipped. For colocalization studies with VEGF, slides were incubated in a mixture of the mAb VEGF (1:200) and isolectin B_4 (1:100), followed by incubation with the AlexaFluor 568 goat anti–mouse secondary IgG (1:250; Invitrogen). Slides were photographed using a confocal laser scanning microscope (LSM 510; Zeiss, Oberkochen, Germany).

Fluorescein Angiography

Fluorescein angiography (FA) was used to visualize changes in retinal vasculature with increasing age in *Nrl*$^{-/-}$, *Nrl*$^{-/-}$*Grk1*$^{-/-}$, C57/Bl6J, and *Grk1*$^{-/-}$ mice. *Nrl*$^{-/-}$ and *Nrl*$^{-/-}$*Grk1*$^{-/-}$ mice were examined from 1, 3, 5, and 7 months of age, and C57/Bl6J and *Grk1*$^{-/-}$ mice were examined at 1 and 7 months of age. Before anesthesia, pupils were dilated with topical phenylephrine HCl (2.5%) and tropicamide (0.5%). After dilation, the mice were anesthetized with intraperitoneal injection of ketamine HCl (100 mg/kg body weight) and xylazine HCl (10 mg/kg body weight) and were kept on a heating pad for the duration of the experiment. The mice were placed in lateral recumbence with the visual axis of the eye upward. The focal axis of the hand-held camera (small animal camera; Kowa Genesis, Tokyo, Japan) was aligned with the visual axis of the mouse. Intraperitoneal injection of 0.05 mL of 10% sodium fluorescein dye solution (Akorn, Buffalo Grove, IL) was administered at the same time imaging (Dataphot; Carl Zeiss; internal time) was started (Vk02 2.11 Digital Imaging for Genesis; Kowa, Torrance, CA). Time-lapse digital photographs were taken of the center, top, bottom, left, and right quadrant for every time point at approximately 1, 3, 5, and 7 minutes after injection.

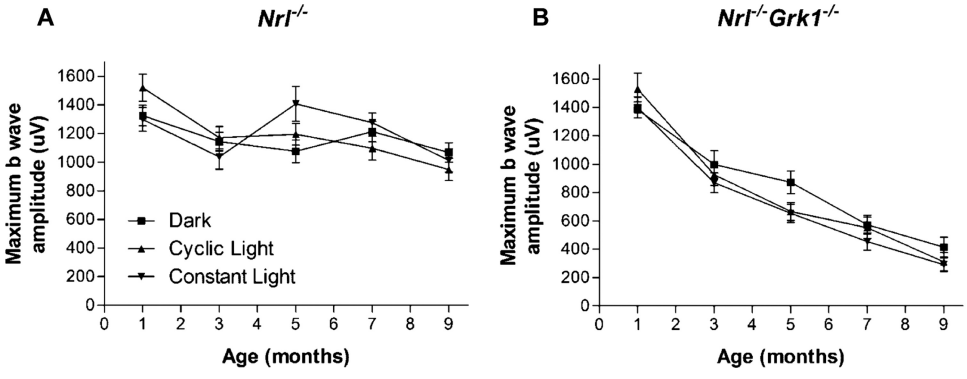

FIGURE 1. Maximum b-wave amplitude of dark-adapted ERG responses in (**A**) *Nrl*$^{-/-}$ and (**B**) *Nrl*$^{-/-}$*Grk1*$^{-/-}$ mice. Mice were dark adapted overnight before ERG recordings. Maximum responses were elicited by high-intensity white fluorescent light. Note the rapid decrease of b-wave amplitude (approximately 40% from 1 to 3 months) with increasing age in the *Nrl*$^{-/-}$*Grk1*$^{-/-}$ mouse reared in the dark, in cyclic light, or in constant light.

RESULTS

Age-Related Light-Independent Cone Dystrophy

ERG analyses of retinal physiology and photopic function show that the b-wave amplitudes of dark-adapted ERG responses elicited by maximum light stimulus are largely stable until 7 months of age in *Nrl*$^{-/-}$ mice, regardless of the animals' environmental lighting conditions (Fig. 1). In contrast, the photopic b-wave amplitude decreases rapidly in *Nrl*$^{-/-}$*Grk1*$^{-/-}$ mice in an age-dependent manner, with a 40% reduction in b-wave amplitude by 3 months of age (Fig. 1B). Importantly, the average b-wave amplitudes of 1-month-old *Nrl*$^{-/-}$*Grk1*$^{-/-}$ mice are similar to those of age-matched *Nrl*$^{-/-}$ controls in the three environmental light conditions tested (Fig. 1B). The ERG results illustrate a defect in cone function and suggest that the degeneration of cone photoreceptors in the *Nrl*$^{-/-}$*Grk1*$^{-/-}$ retina are related to increasing age under different light exposure, in contrast to the light-induced rod degeneration observed in the *Grk1*$^{-/-}$ mouse retina.[14]

Age-matched retinas of light-adapted *Nrl*$^{-/-}$ and *Nrl*$^{-/-}$*Grk1*$^{-/-}$ mice have a similar photoreceptor ONL thickness at 1 month (Figs. 2A, 2D); however, the *Nrl*$^{-/-}$*Grk1*$^{-/-}$ retinas had fewer rosettes and whorls at this age. At 5 months and older, the ONL appears thinner in the *Nrl*$^{-/-}$*Grk1*$^{-/-}$ mouse retina (Figs. 2E, 2F).[15] Cone-specific Arr4 immunoreactivity and H&E staining confirm that the thinning of the retina in 5- and 9-month-old *Nrl*$^{-/-}$*Grk1*$^{-/-}$ mice is the result of cone photoreceptor loss (Figs. 2G–L).

Retinal cross-sections from *Nrl*$^{-/-}$ and *Nrl*$^{-/-}$*Grk1*$^{-/-}$ retinas were immunohistologically stained with pAB S- and M-opsin antibodies and confirmed our previous observations[15] that both S and M cones degenerate in the *Nrl*$^{-/-}$*Grk1*$^{-/-}$ mouse retina in an age-dependent manner (Supplementary Fig. S1; Supplementary Figures and Tables available at http://www.iovs.org/content/51/12/6196/suppl/DC1). By 9 months of age, a significant loss of S- and M-opsin–expressing cones is observed in the *Nrl*$^{-/-}$*Grk1*$^{-/-}$ retinas compared with their age-matched *Nrl*$^{-/-}$ controls. Interestingly, more rosette structures are observed in the ONL of the *Nrl*$^{-/-}$ retina, which are reduced with age faster in *Nrl*$^{-/-}$*Grk1*$^{-/-}$ retinas (Supplementary Fig. S1).

Apoptosis of Cone Photoreceptors

TUNEL analysis was performed on frozen retinal sections from P21 and P30 C57/Bl6J (C57), *Nrl*$^{-/-}$, and *Nrl*$^{-/-}$*Grk1*$^{-/-}$ mice born and raised in cyclic ambient light to further characterize photoreceptor degeneration. A representative picture of a segment from P21 *Nrl*$^{-/-}$*Grk1*$^{-/-}$ and P30 *Nrl*$^{-/-}$ and *Nrl*$^{-/-}$*Grk1*$^{-/-}$ retinal sections demonstrate that apoptotic cells were observed only in the ONL of both *Nrl*$^{-/-}$ and *Nrl*$^{-/-}$*Grk1*$^{-/-}$ mice (Figs. 3A–C) and were statistically significantly different from *Nrl*$^{-/-}$ mice at P30 but not at P21 (Fig. 3D). On quantification of TUNEL-positive cells and repeated-measures ANOVA with Bonferroni correction, the *Nrl*$^{-/-}$ mouse retina was found to have significantly more apoptotic cells than C57 control retinas at both P21 and P30, which is consistent with the slower retinal degeneration phenotype ($P < 0.05$).[1] However, the *Nrl*$^{-/-}$*Grk1*$^{-/-}$ retina shows a statistically significantly greater number of apoptotic cells compared with both *Nrl*$^{-/-}$ ($P < 0.01$) and C57 ($P < 0.001$) controls at P30 but was only significantly different from C57 mice at P21. These results suggest that the cone photoreceptors of these mice die through apoptosis, and the degeneration is exacerbated after ablation of Grk1 that is slightly higher at P21 but is only significantly higher by P30.

Microarray and Ingenuity Pathway Analysis

To identify potential cellular pathways involved in the cone dystrophy in the *Nrl*$^{-/-}$*Grk1*$^{-/-}$ mouse, we performed microarray analysis in triplicate and analyzed our results using statistical analysis software (Genomic Suite; Partek) and IPA. The data reveal statistically significant differences ($P \leq 0.005$) and average fold changes (AFCs) $\geq$1.2 of 422 mapped genes using two-way ANOVA (Supplementary Table S1). The genes with statistically significant upregulation and an AFC $<$2.5 are listed in Table 1, the statistically significantly downregulated genes with an AFC less than -3.0 are listed in Table 2. Expression of 10 known genes (pituitary tumor transforming gene 1, *Pttg1;* tetratricopeptide repeat domain, *28Ttc28;* solute carrier family 6 [proline IMINO transporter], member 20, *Slc6a20;* Ubxn4 UBX domain protein 4, *Ubxn4;* Fanconi anemia, complementation group C, *Fancc;* adenylate cyclase-associated protein 1, *Cap1;* kallikrein 2, *Klk2;* sorbin and SH3 domain containing 1, *Sorbs;* coiled-coil domain containing 21, *Ccdc21;* transmembrane protein 30A, *Tmem30A*) was significantly in-

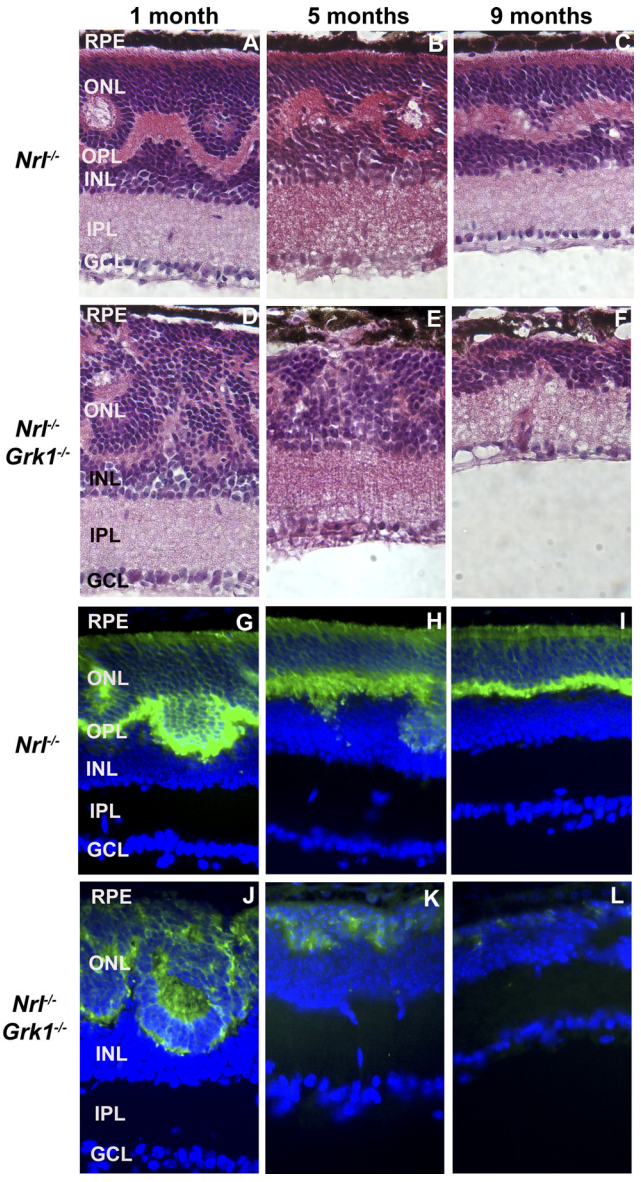

FIGURE 2. Age-dependent cone photoreceptor degeneration in the *Nrl*$^{-/-}$ and *Nrl*$^{-/-}$*Grk1*$^{-/-}$ mouse retina. Retinal sections were (**A–F**) stained with H&E or (**G–L**) immunostained with anti–mCAR-LUMIJ, followed by a fluorescein-conjugated anti–rabbit IgG secondary antibody. Significant thinning of the ONL is observed at 5 months, with complete loss of cones by 9 months. Photographs were taken from the central inferior region of the retina.

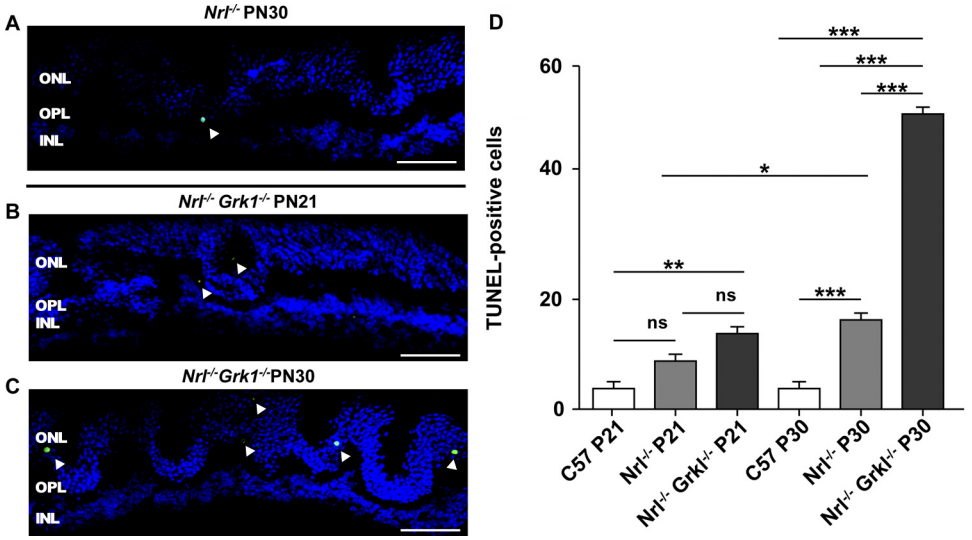

FIGURE 3. TUNEL staining is enhanced in $Nrl^{-/-}Grk1^{-/-}$. Retinal sections from (**A**) P30 $Nrl^{-/-}$, (**B**) P21 $Nrl^{-/-}Grk1^{-/-}$, and (**C**) P30 $Nrl^{-/-}Grk1^{-/-}$ mice were processed for TUNEL staining. Shown are images of the middle superior region of the retina. TUNEL-positive apoptotic cells (*green*) were counted under a fluorescence light microscope. The total number of TUNEL-positive cells from three sections of each mouse was recorded, and the average count (mean ± SEM) was calculated from three mice using one-way ANOVA of the same genotype (**D**). $^{*}P < 0.05$; $^{**}P < 0.01$; $^{***}P < 0.001$. Scale bar, 20 μm.

creased in the $Nrl^{-/-}Grk1^{-/-}$ compared with the $Nrl^{-/-}$ group. On examination of the transcripts with the highest fold increases, *Pttg1* appears twice with a 130.7- and 70.0-fold increase (Table 1). The *Pttg1* gene encodes for a transcription regulatory protein that can shuttle between the cytoplasm and nucleus with alternative roles in sister chromatid segregation.[23] Interestingly, Crumbs homolog 1 (*Crb1*) transcript levels were decreased in $Nrl^{-/-}Grk1^{-/-}$ mice approximately −6.3-fold compared with $Nrl^{-/-}$ mice. This deregulation of *Crb1* and *Pttg1* has been observed in two separate photoreceptor dystrophy models, the Crb1- and Ras protein-specific guanine nucleotide releasing factor 1 (RasGRF1) null mutant mice, both of which demonstrate dystrophic retinas and are proposed models for retinal disease studies.[23,24] *Klk2,* with a fold increase of 29.7, was also examined because of its serine protease and autoantigenic functions and was recently identified as a major contributor in an experimental model for autoimmune keratoconjunctivitis sicca in Lewis rats.[25]

Other genes of interest that were significantly deregulated include the RNA-binding protein embryonic lethal, abnormal vision, *Drosophila*-like-1 (Hu-antigen R) (*Elavl1*) (AFC, −6.99) known to play crucial roles in the stabilization and transport mRNA, including vascular endothelial growth factor (*VEGF*).[26] Similarly, Usher syndrome 1C (autosomal recessive, severe) (*Ush1C*) (AFC-4.84) encodes for harmonin, a PDZ domain-containing protein with isoforms synthesized and expressed in photoreceptors.[27,28] Patients with mutations in USH1C have abnormal rod and cone findings on electroretinography and retinal degeneration at an early age.

Transcripts were categorized using IPA according to biological function with respect to diseases and disorders, molecular and cellular functions, and physiological system development and function. Of these pathways, neurologic disease, cell sig-

TABLE 1. Comparison of Upregulated Transcripts between $Nrl^{-/-}Grk1^{-/-}$ and $Nrl^{-/-}$ Retinas

Symbol	Entrez Gene Name	*P*	Fold Change	ProbeSet ID
Pttg1	Pituitary tumor-transforming 1	2.85E−05	130.741	1438390_s_at
Pttg1	Pituitary tumor-transforming 1	2.13E−06	70.022	1424105_a_at
Cap1	CAP, adenylate cyclase-associated protein 1 (yeast)	2.39E−05	32.933	1417461_at
Klk2	Kallikrein-related peptidase 2	4.01E−05	29.665	1425182_x_at
Cap1	CAP, adenylate cyclase-associated protein 1 (yeast)	4.13E−05	23.502	1417462_at
Lancl3	LanC lantibiotic synthetase component C-like 3 (bacterial)	1.43E−04	19.525	1437268_at
A330076H08RIK	RIKEN cDNA A330076H08 gene	1.69E−03	9.575	1457557_at
Nudt19	Nudix (nucleoside diphosphate linked moiety X)-type motif 19	7.10E−04	7.046	1434216_a_at
Dhdh	Dihydrodiol dehydrogenase (dimeric)	1.32E−03	6.802	1453487_at
4833408G04RIK	RIKEN cDNA 4833408G04 gene	4.20E−03	6.083	1454409_at
Actg2	Actin, gamma 2, smooth muscle, enteric	1.29E−03	4.155	1416454_s_at
Osbpl3	Oxysterol binding protein-like 3	2.57E−04	4.146	1438724_at
Actr1A	ARP1 actin-related protein 1 homolog A, centractin alpha (yeast)	1.98E−03	4.016	1457970_at
Lgals4	Lectin, galactoside-binding, soluble, 4	5.43E−04	3.480	1451336_at
AY512938	cDNA sequence AY512938	4.15E−03	3.468	1458551_at
Cyp26a1	Cytochrome P450, family 26, subfamily A, polypeptide 1	1.80E−03	3.374	1419430_at
Ociad1	OCIA domain containing 1	1.29E−03	3.339	1424952_at
Nudt19	Nudix (nucleoside diphosphate linked moiety X)-type motif 19	2.96E−04	3.337	1432332_a_at
Ublcp1	Ubiquitin-like domain containing CTD phosphatase 1	4.69E−03	3.165	1429606_at
Slc6a20	Solute carrier family 6 (proline IMINO transporter), member 20	1.32E−05	3.117	1427221_at
2810488G03RIK	RIKEN cDNA 2810488G03 gene	1.74E−03	2.927	1429068_at
Gsto1	Glutathione S-transferase omega 1	2.09E−03	2.728	1456036_x_at
Myom2	Myomesin (M-protein) 2, 165 kDa	2.13E−03	2.714	1457435_x_at
Ankrd11	Ankyrin repeat domain 11	1.28E−03	2.694	1436967_at
Itga6	Integrin, alpha 6	1.45E−03	2.531	1422444_at

TABLE 2. Comparison of Downregulated Transcripts between *Nrl*$^{-/-}$*Grk1*$^{-/-}$ and *Nrl*$^{-/-}$ Retinas

Symbol	Entrez Gene Name	*P*	Fold Change	ProbeSet ID
Grk1	G protein-coupled receptor kinase 1	9.36E−04	−72.593	1421361_at
Znf26	Zinc finger protein 26	3.73E−04	−30.101	1444092_at
Zfp874	Zinc finger protein 874	2.13E−04	−29.670	1434171_at
Skiv2l2	Superkiller viralicidic activity 2-like 2 (*Saccharomyces cerevisiae*)	1.48E−04	−28.664	1447517_at
9430027B09RIK	RIKEN cDNA 9430027B09 gene	2.64E−03	−21.358	1454232_at
Mtmr7	Myotubularin-related protein 7	1.67E−03	−19.189	1447831_s_at
Rbm45	RNA-binding motif protein 45	1.97E−03	−12.899	1437904_at
Abcb10	ATP-binding cassette, subfamily B (MDR/TAP), member 10	2.15E−03	−11.188	1416403_at
Dcdc2B	Doublecortin domain-containing 2B	2.18E−03	−9.736	1444714_at
Map2k7	Mitogen-activated protein kinase kinase 7	1.36E−03	−9.381	1457182_at
C4orf47	Chromosome 4 open reading frame 47	2.31E−05	−8.472	1453168_at
Yipf4	Yip1 domain family, member 4	3.40E−03	−8.031	1426417_at
Elavl1	ELAV (embryonic lethal, abnormal vision, *Drosophila*)-like 1 (Hu antigen R)	5.84E−04	−6.986	1440464_at
Crb1	Crumbs homolog 1 (*Drosophila*)	1.03E−03	−6.324	1441330_at
Esco1	Establishment of cohesion 1 homolog 1 (*S. cerevisiae*)	2.18E−04	−6.056	1424324_at
AI605517	Expressed sequence AI605517	2.29E−03	−6.042	1457797_at
Ush1c	Usher syndrome 1C (autosomal recessive, severe)	1.19E−03	−4.839	1450001_a_at
Fkbp9	FK506 binding protein 9, 63 kDa	1.02E−03	−4.767	1423677_at
4632415L05RIK	RRS1 ribosome biogenesis regulator homolog pseudogene	3.91E−03	−4.689	1419611_at
C8orf41	Chromosome 8 open reading frame 41	3.77E−03	−4.650	1435309_at
Fut10	Fucosyltransferase 10 (alpha (1,3) fucosyltransferase)	3.29E−03	−4.601	1437388_at
Pik3ap1	Phosphoinositide-3-kinase adaptor protein 1	2.20E−03	−4.017	1429831_at
4933439C20RIK	Phosphatidylserine decarboxylase, pseudogene 1	6.42E−05	−3.843	1435353_a_at
Als2	Amyotrophic lateral sclerosis 2 (juvenile)	9.83E−04	−3.813	1417784_at
Rnls	Renalase, FAD-dependent amine oxidase	3.40E−03	−3.510	1453180_at
Mogat1	Monoacylglycerol O-acyltransferase 1	2.54E−03	−3.350	1419504_at
Nek3	NIMA (never in mitosis gene a)-related kinase 3	1.56E−03	−3.326	1418947_at

naling, and nervous system development and function were ranked as the top categories according to *P* value and number of molecules categorized (Supplementary Table S2). The top canonical pathway identified was the oncostatin M signaling pathway (*P* value 3.51×10^{-3}), which activates the Janus kinase (JAK)-signal transducer and activator of transcription 1 (STAT) signaling machinery in some retinal degenerative disease models.[23,29] Other key canonical pathways associated with the *Nrl*$^{-/-}$*Grk1*$^{-/-}$ retinal dystrophy model include Synaptic Long-Term Potentiation Signaling, the Pentose Phosphate Pathway, Rac signaling, and Ciliary Neurotrophic factor (Cntf) Signaling (Supplementary Fig. S2). The top networks identified with their respective number of focus molecules are presented in Supplementary Table S3. Of these identified networks, the Inflammatory Disease, Inflammatory Response network was the most relevant to our model system because of its known association with choroidal neovascularization. The upregulated transcripts from this network were organized into a schematic diagram and are presented in Figure 4. Interestingly, upregulation of Klk2 was identified in this pathway, as was the Oncostatin M signaling cascade with increased transcription of Stat1 along with other inflammatory response genes.

Confirmation of the Gene Expression Changes by Quantitative PCR

Quantitative PCR was performed for select genes of interest, *Pttg1* and *Klk2,* (Fig. 5) to validate the microarray results (Supplementary Table S1), and similar significant increases in both transcripts were observed compared with the β-actin reference standard. Notably, a similar trend in upregulation of both transcripts was observed in *Grk1*$^{-/-}$ compared with WT retinas.

Neovascularization

The identification of the Inflammatory Disease, Inflammatory Response Network by IPA as one of the top networks led us to examine *Nrl*$^{-/-}$*Grk1*$^{-/-}$ retinas for neovascularization as a contributor to cone photoreceptor cell death because of its association with CNV. Endothelial cell staining using isolectin B_4 and neovascularization testing using FA were performed to analyze changes in retinal vasculature with increasing age. Isolectin B_4 staining (green) was observed in the inner nuclear layer (INL) and inner plexiform layer (IPL) in 1-month-old *Nrl*$^{-/-}$ mice (Fig. 6). The morphology and retinal vasculature are similar to those of healthy retinas and are consistent throughout the entire section of *Nrl*$^{-/-}$ controls. Age-matched *Nrl*$^{-/-}$*Grk1*$^{-/-}$ mice reared under the same lighting conditions, however, exhibit choroidal anastomoses that infiltrate the retinal pigment epithelium (RPE). Blood vessels are present in the choroid, INL, outer plexiform layer (OPL), IPL, and inner limiting membrane (ILM). Compared with the controls, *Nrl*$^{-/-}$*Grk1*$^{-/-}$ mice have atrophied RPE cells and breaks in the RPE monolayer coupled with anastomoses forming from both the choroid and the inner retina (Fig. 6). These studies demonstrate that by 1 month of age, *Nrl*$^{-/-}$*Grk1*$^{-/-}$ retinas have blood vessel infiltration that penetrates all retinal layers (Fig. 6).

To correlate the observed photoreceptor TUNEL staining with choroidal anastomoses, we performed isolectin B_4 IHC on retinal sections of P21 *Nrl*$^{-/-}$*Grk1*$^{-/-}$ mice and compared them with P30 *Nrl*$^{-/-}$*Grk1*$^{-/-}$ sections. Supplementary Figure S3 demonstrates that overall, these mice have less blood vessel penetration from the choriocapillaris and have an unbroken RPE monolayer, although signs of the initial penetration of blood vessels at this age were present (Supplementary Fig. S3, top panel).

VEGF is a hypoxia-induced cytokine that is strongly implicated in angiogenesis by virtue of its absolute requirement for retinal vascularization and its expression in spatial and temporal conjunction with developing retinal blood vessels.[30] Therefore, IHC staining using an anti-VEGF antibody on P21 *Nrl*$^{-/-}$ and *Nrl*$^{-/-}$*Grk1*$^{-/-}$ retinas was performed. The level of VEGF

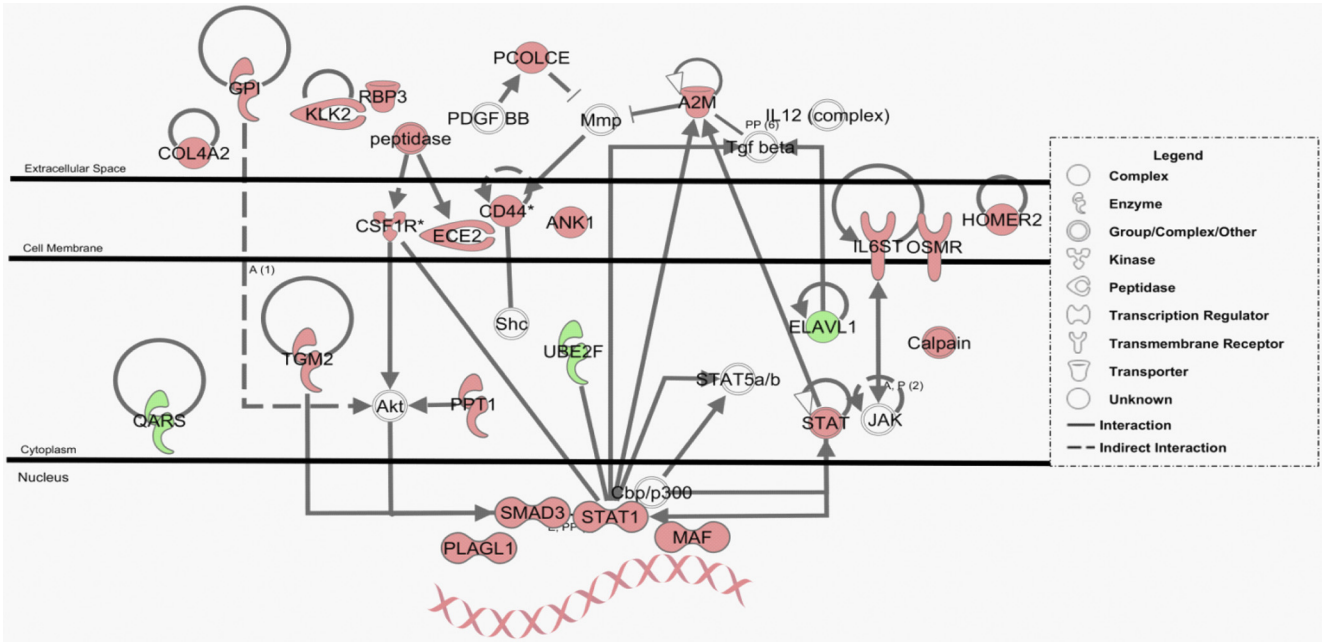

FIGURE 4. Schematic representation of the inflammatory disease, inflammatory response network. Microarray data set analysis was used to generate a hypothetical network based on upregulated transcripts. *Dotted lines*: indirect protein relationships. *Solid lines*: direct relationships, including protein-protein interactions, phosphorylation, activation, and ligand receptor binding. *Red molecules* represent significantly upregulated transcripts. *Green molecules* represent downregulated transcripts. *Uncolored molecules* were not differentially expressed but were important components of the network.

expression in P21 $Nrl^{-/-}Grk1^{-/-}$ mice is more apparent than the staining pattern observed in $Nrl^{-/-}$ mice of the same age (Fig. 7A). A control section without the primary antibody was performed to confirm that staining was not due to secondary background (data not shown). These results indicate an enhanced level of VEGF expression in $Nrl^{-/-}Grk1^{-/-}$ mice that begins as early as P21. The section was focused on the nuclear plane; however, VEGF expression was localized throughout the retinal section but was highest in the ILM located below the IPL.

A higher magnification image of VEGF expression in the endothelial cells of a P21 $Nrl^{-/-}Grk1^{-/-}$ retina is provided in Figure 7B. The staining pattern indicates that VEGF levels are enhanced and highly expressed near the blood vessels of these mice, particularly in the branching segments of the vessel. Age-matched $Nrl^{-/-}$ mice did not exhibit VEGF expression within their blood vessels (Fig. 7A).

Gross progressive changes that occur as a consequence of blood vessel penetration were examined using FA on $Nrl^{-/-}$ and $Nrl^{-/-}Grk1^{-/-}$ mice at 1, 3, 5, and 7 months of age. $Nrl^{-/-}$ mice exhibit no detectable leakage and have healthy retinal vasculature at all ages examined (Fig. 8). In contrast, age-matched $Nrl^{-/-}Grk1^{-/-}$ mice have a moderate level of leakage beginning at 1 month in the right upper quadrant (arrows), and by 3 months an excessive amount of leakage is observed that progresses with age (Fig. 8). FA staining on P21 $Nrl^{-/-}Grk1^{-/-}$ mice could not be performed because of their small size. Leakage is first noticed in the right quadrant and spreads throughout the retina by 5 months (data not shown). Conversely, the retinas of C57 and $Grk1^{-/-}$ mice at both 1 month and 7 months of age demonstrate healthy vasculature in all animals tested (Supplementary Fig. S4).

DISCUSSION

The absence of Grk1 in retinas leads to a rapid light-dependent retinal degeneration of rod photoreceptors because of a defec-

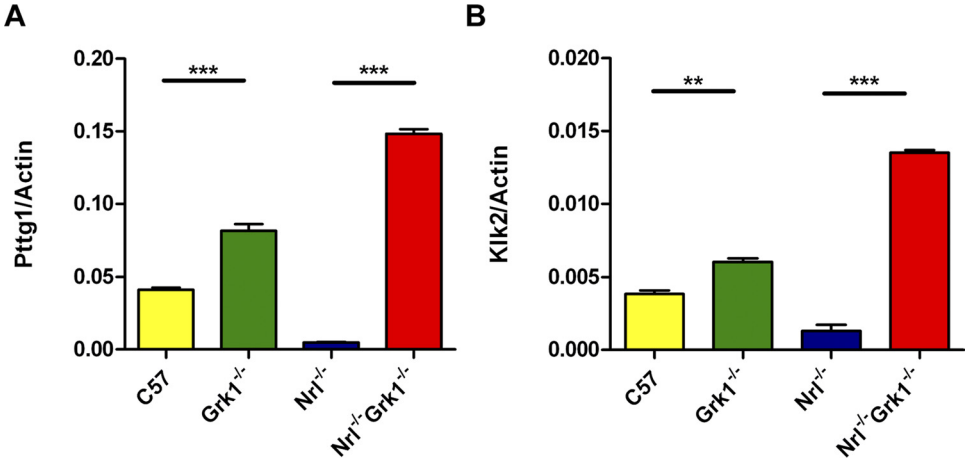

FIGURE 5. Confirmation of differential mRNA expression of *Klk2 and Pttg1* using quantitative RT-PCR. cDNAs from WT, $Grk1^{-/-}$, $Nrl^{-/-}$, and $Nrl^{-/-}Grk1^{-/-}$ 1-month-old retinas were used for quantitative expression analysis, and β-actin was a reference standard. Statistically significant upregulation of (**A**) *Pttg1* and (**B**) *Klk2* was observed in both $Grk1^{-/-}$ compared with WT and $Nrl^{-/-}Grk1^{-/-}$ compared with $Nrl^{-/-}$. $^{*}P < 0.05$; $^{**}P < 0.01$.

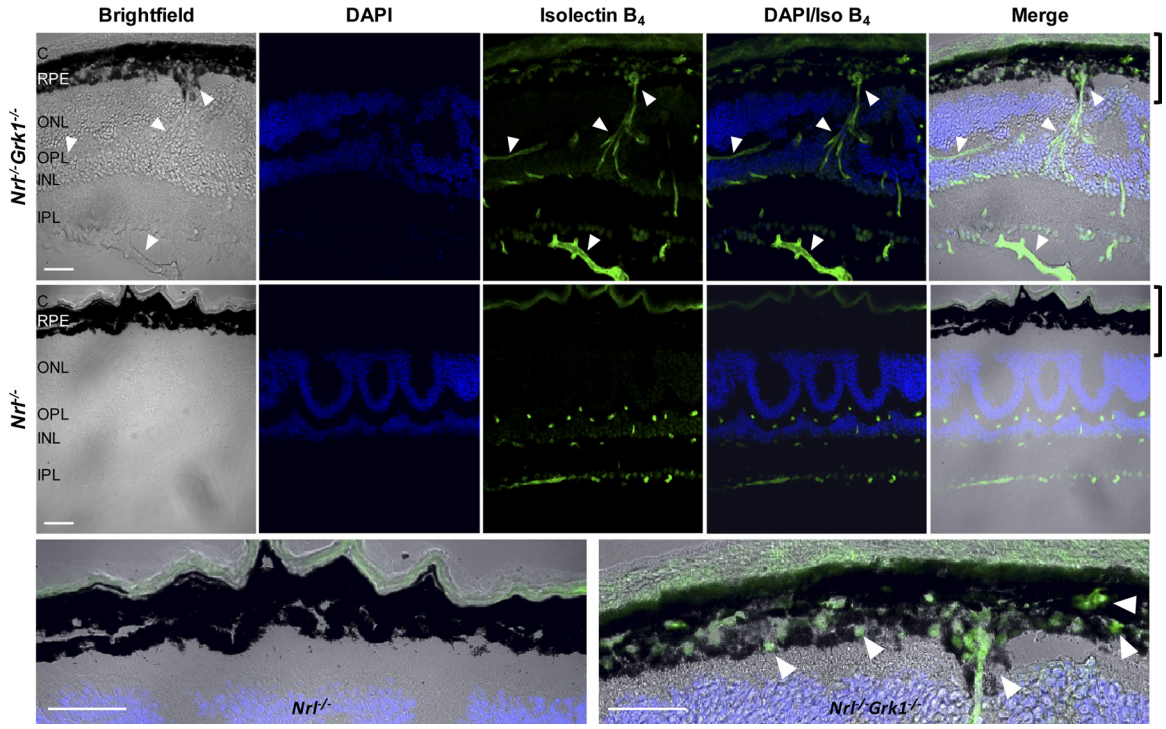

FIGURE 6. Retinal anastomoses in *Nrl*$^{-/-}$*Grk1*$^{-/-}$ mice. Retinas were harvested from 1-month-old *Nrl*$^{-/-}$ and *Nrl*$^{-/-}$*Grk1*$^{-/-}$ mice raised in cyclic light. *Top*: *Nrl*$^{-/-}$*Grk1*$^{-/-}$ retina. *Middle*: *Nrl*$^{-/-}$ control. *Bottom*: Magnification of the RPE from merged images of *Nrl*$^{-/-}$ (*left*) and *Nrl*$^{-/-}$*Grk1*$^{-/-}$ (*right*). Bright-field images demonstrate changes in the RPE structure (*arrows*). DAPI is used as a nuclear stain (*blue*), and fluorescein-labeled GSL isolectin B_4 (*green*) shows penetration of blood vessels into the retina from the choroid (*arrows*) in *Nrl*$^{-/-}$*Grk1*$^{-/-}$. C, choroid. Scale bar, 20 μm. Images were taken with a confocal laser scanning microscope using a 40× lens.

tive shutoff of rhodopsin in phototransduction.[14] Moreover, Grk1 null mice have a delayed recovery of photopic response in both the rod-dominant[5] and the "all-cone" *Nrl*$^{-/-}$ mouse retina.[3,15] In this study, we observed for the first time that the cone photoreceptors of *Nrl*$^{-/-}$ mice lacking Grk1 expression degenerate with increasing age in a manner that is independent of their environmental light exposure (Fig. 1). Furthermore, we established that even when the *Nrl*$^{-/-}$*Grk1*$^{-/-}$ mice are maintained in darkness, their retinas exhibit cone functional deficits and slower morphologic changes leading to the inevitable loss of the nuclei in the ONL (Fig. 2). The first indication of a defective photopic ERG function was apparent at 3 months in mice reared in all lighting conditions tested and led us to examine the molecular and morphologic changes at 1 month, when photopic ERG responses are similar to those of *Nrl*$^{-/-}$ controls (Fig. 1). Despite the well-characterized essential function in phototransduction recovery of Grk1, our data suggest alternative functions for Grk1, either directly or indirectly, in the homeostasis and survival of cone photoreceptors. Our results strongly suggest that even with a defective phototransduction shutoff pathway, the *Nrl*$^{-/-}$ mice are resistant to light-mediated damage, and the cone dystrophy is a manifestation of an alternative mechanism.

In most retinal degeneration (rd) models, cone cell death is often secondary to rod cell death because of the release of endotoxins from degenerating rods, environmental alterations, or deprivation of a rod-derived trophic factor.[31] The loss of cone function, however, results in the more severe disability and reduction in visual quality. We believe that the differences found between the *Grk1*$^{-/-}$ and *Nrl*$^{-/-}$*Grk1*$^{-/-}$ phenotypes are a demonstration of the dynamic role and protective mechanisms rods use in the prevention of cone cell death.

Grk1 expression is essential for light-dependent phosphorylation of SWL and medium wavelength (MWL) pigments in the mouse retina[8] and controls the rapid rate of cone recovery analogous to its rod function.[3,5,15] Immunohistochemical studies using antibodies for S- or M-opsin plus Arr4 prove that both SWL- and MWL-expressing cones degenerate with increasing age (Fig. 2; Supplementary Fig. S1). Furthermore, quantification of TUNEL-positive nuclei confirms that the cone photoreceptors have hallmarks of active cell death that are significant by 1 month of age (Fig. 3).

To further characterize the cone dystrophy of *Nrl*$^{-/-}$*Grk1*$^{-/-}$ retinas, vascular cell staining and FA experiments were performed. *Nrl*$^{-/-}$*Grk1*$^{-/-}$ mice harbor breaks in the RPE with retinal anastomoses detectable by 1 month (Fig. 6) and exhibit retinal angiogenesis that progresses with age (Fig. 8). FA staining patterns show first signs of leakage in the right quadrant of the eye, which may explain the wave of cell death in SWL- and MWL-expressing photoreceptors of these mice (Supplementary Fig. S1). In contrast, *Grk1*$^{-/-}$ mice are similar to C57 controls (Supplementary Fig. S4) and do not exhibit a fluorescein dye leakage like that of *Nrl*$^{-/-}$*Grk1*$^{-/-}$ retinas, even by 7 months. This observation recapitulates our findings that the angiogenesis is specific to the loss of Grk1 in *Nrl*$^{-/-}$ retinas, and our observed dystrophy is most likely caused by an increase in retinal angiogenesis and not light exposure.

There are two known types of neovascularization in the retina: retinal neovascularization (RNV) and choroidal neovascularization (CNV). RNV is characterized by sprouting blood vessels that penetrate the ILM and grow into the vitreous,[32] though in some cases the blood vessels can grow in the other direction, from the outer retina to the subretinal space. The pathogenesis of RNV is better understood than that of CNV, with ischemia, VEGF expression, hyperoxia-, and hypoxia-mediated gene regulation the key players in the characterization of the disease.[32] In *Nrl*$^{-/-}$*Grk1*$^{-/-}$ mice, we observed an

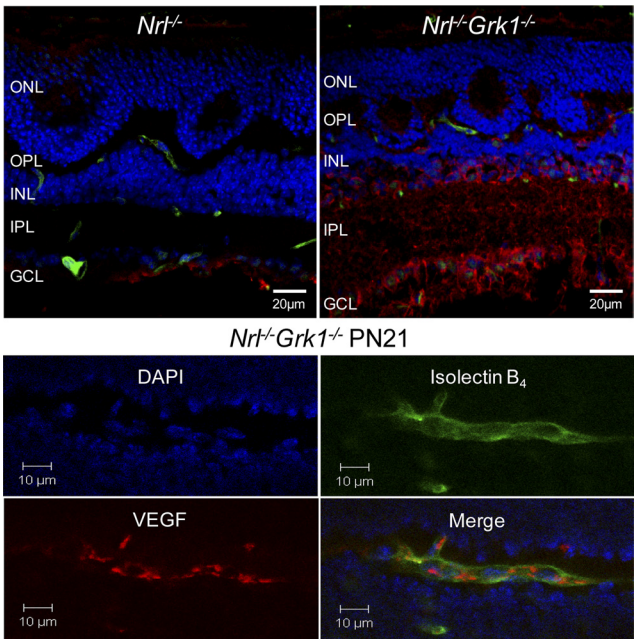

FIGURE 7. VEGF expression is enhanced in $Nrl^{-/-}Grk1^{-/-}$ retinas beginning at P 21. (**A**) Retinas from P21 $Nrl^{-/-}$ and $Nrl^{-/-}Grk1^{-/-}$ mice were costained with isolectin B_4 (*green*) and VEGF (*red*), and DAPI (*blue*) was used for nuclei staining. Images demonstrate an enhanced level of VEGF expression in $Nrl^{-/-}Grk1^{-/-}$ retinas in the OPL, INL, and IPL, whereas minimal staining was observed in the ganglion cell layer below the IPL in the age-matched $Nrl^{-/-}$ section. (**B**) Higher magnification of a blood vessel in the OPL of a P21 $Nrl^{-/-}Grk1^{-/-}$ retina. VEGF is expressed near the sprouting blood vessel, particularly around the branching segments.

enhanced level of VEGF expression beginning at P21 that localized to both the blood vessels and the ILM (Fig. 7).

Alternatively to RNV, the molecular participants in the pathogenesis and stimulation of CNV are less well understood. One possible contributor to CNV is inflammation. Previous reports have indicated that deposits in and around Bruch's membrane may induce the inflammatory response,[32] whereas another attributes CNV to an abnormal extracellular matrix resulting in diffuse thickening of Bruch's membrane.[33] During their initial characterization, $Nrl^{-/-}$ OS discs were often found to misalign and abnormally associate with the RPE,[1] which may contribute to the weakened Bruch's membrane and the increased susceptibility for choroidal blood vessel penetration after an insult, in this case the loss of Grk1. We also observed an increase in the level of inflammatory response genes in our cone dystrophy model at 1 month (Supplementary Table S3; Fig. 6) and a subsequent increase in blood vessel penetration into the retina that was exacerbated with age (Supplementary Fig. S3). After isolectin B_4 staining, we identified blood vessel penetration from the choroid into the retina and the ILM, though it was difficult to determine in which direction the anastomosis was growing in the ILM. Given the results presented in this study, we hypothesize that the loss of Grk1 on the $Nrl^{-/-}$ background stimulates angiogenesis that most closely resembles retinal angiomatous proliferation, which is a variant form of CNV typified by intraretinal neovascularization in the form of a retinal-retinal anastomosis and intraretinal hemorrhage.

Microarray studies are an informative approach in understanding the potential molecular pathways and mechanisms associated with the cone dystrophy and retinal angiogenesis in our double-knockout mice. Our analysis of the top molecular candidates identified by IPA isolated two candidate genes, *Pttg1* and *Klk2,* as interesting targets for their role in cell cycle progression and inflammation, respectively, and their previous identification in other retinal dystrophy mouse models.[23,24] *Pttg1* has the greatest fold increase in the $Nrl^{-/-}Grk1^{-/-}$ retina (Table 1; Fig. 5A) and was of interest because of its deregulation in both Crb1 and RasGRF1 null mice.[23,24] Crb1 mutant and null mice exhibit defects in retinal morphology and focal retinal disorganization, and humans with mutations in Crb1 develop Leber congenital amaurosis.[23] RasGRF1 null mice, which have severe light perception defects, also differentially express both *Pttg1* and *Crb1* genes, among other transcripts.[24] Similarly, the $Nrl^{-/-}Grk1^{-/-}$ retinas exhibit a decrease in expression of *Crb1* by more than sixfold (Table 2). *Klk2*, with an up-regulation of more than 29-fold that was validated by qPCR (Table 1; Fig. 5B), is an autoantigen that was recently described as an inducer of Sjögren's syndrome-like keratoconjunctivitis sicca in Lewis rats.[25] Tissue kallikreins inhibit apoptosis and promote cell survival though the activation of the mitogen-activated protein kinases $p44^{ERK1}$ and $p42^{ERK2}$ (Erk1/2) signaling pathways.[34] We believe that the upregulation of Klk2 and Pttg1 is noteworthy because of the high AFC values for each and for their prevalence in microarray studies from other mouse models of retinal degenerative disease; nevertheless, the precise role and causal mechanisms behind differential expression of these transcripts require further study.

Oncostatin M signaling was the top pathway identified (Supplementary Fig. S2) and is a well-characterized mechanism for both light-mediated and inherited forms of retinal degeneration.[29] Previously, the retinal degeneration 1 (*rd1*) mouse, with a mutation in the β-subunit of phosphodiesterase leading to a rapid degeneration of photoreceptors, and the VPP mouse, a transgenic strain carrying three rhodopsin mutations (V20G, P23H, P27L) leading to a slow degeneration,[35] were examined for JAK-STAT signaling as independent forms of inherited retinal degeneration.[29] Phosphorylation of STAT3 and viral proto-oncogene 1 (Akt), along with an induction of leukemia inhib-

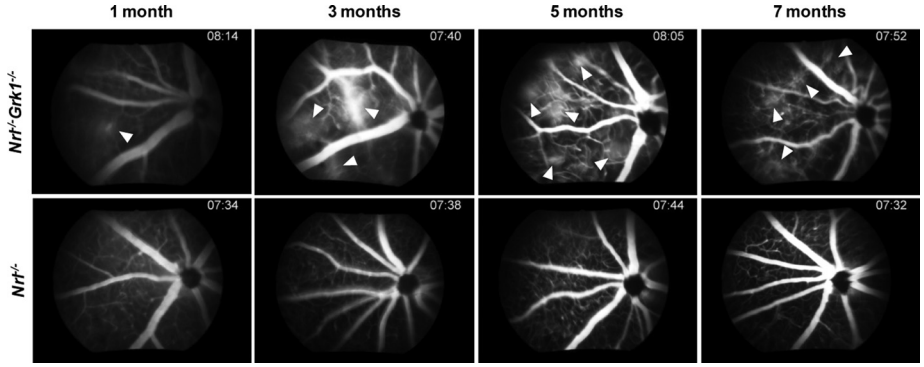

FIGURE 8. FA staining of $Nrl^{-/-}$ and $Nrl^{-/-}Grk1^{-/-}$ mice. Images represent the right quadrant of the right eye of each animal at 1, 3, 5, and 7 months of age. *Top*: $Nrl^{-/-}Grk1^{-/-}$ retinas. (bottom) $Nrl^{-/-}$ controls. *Arrows*: Leakage of blood vessels in $Nrl^{-/-}Grk1^{-/-}$ mice that begins at 1 month and progresses with age. Retinas from age-matched $Nrl^{-/-}$ mice appear normal with healthy vasculature patterns. Images were taken at approximately 7 minutes after injection of the fluorescein dye.

itory factor (Lif), Cntf, fibroblast growth factor-2, Osmr, Gp130, and Ch3l1, are some of the family members of the oncostatin pathway that are upregulated in both mouse models and can be identified in the immune response pathway found in the *Nrl*$^{-/-}$*Grk1*$^{-/-}$ retina (Tables 1, 2; Fig. 6).[29,36] It is unclear from the microarray and qPCR data which cell types exhibit upregulation or downregulation of the transcripts characterized; however, we postulate that these changes in gene expression are associated in the cone photoreceptor degeneration observed in the *Nrl*$^{-/-}$*Grk1*$^{-/-}$ mouse. We understand the challenging caveats when identifying potential signal transduction pathways using either microarray studies or proteomic approaches because of the volume of information acquired using either technique. However, data presented here lay the groundwork for further studies.

Grk1 is only one of at least seven members of the Grk superfamily expressed in the mouse retina and pineal gland, including Grk2.[37] The ubiquitous Grk2 may be a relevant modulator of inflammatory responses because of its ability to attenuate chemokine-induced migration in T cells and monocytes.[38] Chronic downregulation in Grk2 protein expression in immune cells leads to an aberrant inflammatory response.[37] Despite the limitations of studying a model that does not mimic the natural structure of a rod-dominant retina, the *Nrl*$^{-/-}$*Grk1*$^{-/-}$ mouse is an invaluable tool that demonstrates the relevance of Grk1 in cones and supports the theory that Grk1 has alternative roles in the retina, analogous to Grk2, in the regulation of inflammatory response genes in maintaining healthy cone structure and function.

In conclusion, we have identified a retinal neovascularization phenotype that most closely resembles retinal angiomatous proliferation in AMD. Although future studies are required, our working hypothesis is that Grk1 ablation in cones leads to a hypoxic or metabolically compromised environment that subsequently stimulates increased blood vessel penetration into the retina, leading to increased cone apoptosis. It is important to note that the OS discs of *Nrl*$^{-/-}$ mice have been characterized to misalign and abnormally associate with the RPE monolayer,[1] which may facilitate blood vessel penetration by way of a weakened Bruch's membrane. Closer inspection of the membrane itself must be conducted to further examine this possibility. Forthcoming studies will extrapolate the causal relationship and relevance of Grk1 in the cone photoreceptor and will provide a model for potential pharmacologic interventions to either slow or rescue photoreceptors from cell death.

Acknowledgments

The authors thank Mary D. Allen for her generous continued support for their vision research program; Yibu Chen (Bioinformatics Service Program, USC Norris Medical Library) for assistance with the microarray analysis; Lawrence Rife, Fernando Gallardo, Xuemei Zhu, Kebin Wu, and Ernesto Barron for technical support; Christina Ma, Samyukta Mullangi, and Alexander Wang for assistance with experiments; Shun-Ping Huang and Freddi Isaac Zuniga for contributions and support; Anand Swaroop and Alan Mears for generously providing the *Nrl*$^{-/-}$ mice; and Ching-Kang Jason Chen for the *Grk1*$^{-/-}$ mice.

References

1. Mears AJ, Kondo M, Swain PK, et al. Nrl is required for rod photoreceptor development. *Nat Genet.* 2001;29:447–452.
2. Yoshida S, Mears AJ, Friedman JS, et al. Expression profiling of the developing and mature Nrl$^{-/-}$ mouse retina: identification of retinal disease candidates and transcriptional regulatory targets of Nrl. *Hum Mol Genet.* 2004;13:1487–1503.
3. Nikonov SS, Daniele LL, Zhu X, Craft CM, Swaroop A, Pugh EN Jr. Photoreceptors of Nrl$^{-/-}$ mice coexpress functional S- and M-cone opsins having distinct inactivation mechanisms. *J Gen Physiol.* 2005;125:287–304.
4. Daniele LL, Lillo C, Lyubarsky AL, et al. Cone-like morphological, molecular, and electrophysiological features of the photoreceptors of the Nrl knockout mouse. *Invest Ophthalmol Vis Sci.* 2005;46:2156–2167.
5. Lyubarsky AL, Chen C, Simon MI, Pugh EN Jr. Mice lacking G-protein receptor kinase 1 have profoundly slowed recovery of cone-driven retinal responses. *J Neurosci.* 2000;20:2209–2217.
6. Weiss ER, Ducceschi MH, Horner TJ, Li A, Craft CM, Osawa S. Species-specific differences in expression of G-protein-coupled receptor kinase (GRK) 7 and GRK1 in mammalian cone photoreceptor cells: implications for cone cell phototransduction. *J Neurosci.* 2001;21:9175–9184.
7. Zhao X, Huang J, Khani SC, Palczewski K. Molecular forms of human rhodopsin kinase (GRK1). *J Biol Chem.* 1998;273:5124–5131.
8. Zhu X, Brown B, Li A, Mears AJ, Swaroop A, Craft CM. GRK1-dependent phosphorylation of S and M opsins and their binding to cone arrestin during cone phototransduction in the mouse retina. *J Neurosci.* 2003;23:6152–6160.
9. Zhao X, Yokoyama K, Whitten ME, Huang J, Gelb MH, Palczewski K. A novel form of rhodopsin kinase from chicken retina and pineal gland. *FEBS Lett.* 1999;454:115–121.
10. Chen J, Makino CL, Peachey NS, Baylor DA, Simon MI. Mechanisms of rhodopsin inactivation in vivo as revealed by a COOH-terminal truncation mutant. *Science.* 1995;267:374–377.
11. Hisatomi O, Matsuda S, Satoh T, Kotaka S, Imanishi Y, Tokunaga F. A novel subtype of G-protein-coupled receptor kinase, GRK7, in teleost cone photoreceptors. *FEBS Lett.* 1998;424:159–164.
12. Chen CK, Zhang K, Church-Kopish J, et al. Characterization of human GRK7 as a potential cone opsin kinase. *Mol Vis.* 2001;7:305–313.
13. Weiss ER, Raman D, Shirakawa S, et al. The cloning of GRK7, a candidate cone opsin kinase, from cone- and rod-dominant mammalian retinas. *Mol Vis.* 1998;4:27.
14. Chen CK, Burns ME, Spencer M, et al. Abnormal photoresponses and light-induced apoptosis in rods lacking rhodopsin kinase. *Proc Natl Acad Sci U S A.* 1999;96:3718–3722.
15. Zhu X, Brown B, Rife L, Craft CM. Slowed photoresponse recovery and age-related degeneration in cones lacking G protein-coupled receptor kinase 1. In: Hollyfield JG, Anderson RE, LaVail MM, eds. *Advances in Experimental Medicine and Biology*. New York: Springer; 2006:133–139.
16. Zhu X, Li A, Brown B, Weiss ER, Osawa S, Craft CM. Mouse cone arrestin expression pattern: light-induced translocation in cone photoreceptors. *Mol Vis.* 2002;8:462–471.
17. Zhu X, Wu K, Rife L, et al. Carboxypeptidase E is required for normal synaptic transmission from photoreceptors to the inner retina. *J Neurochem.* 2005;95:1351–1362.
18. Zhu X, Craft CM. Modulation of CRX transactivation activity by phosducin isoforms. *Mol Cell Biol.* 2000;20:5216–5226.
19. Li A, Zhu X, Brown B, Craft CM. Gene expression networks underlying retinoic acid-induced differentiation of human retinoblastoma cells. *Invest Ophthalmol Vis Sci.* 2003;44:996–1007.
20. Wu Z, Irizarry RA. Stochastic models inspired by hybridization theory for short oligonucleotide arrays. *J Comput Biol.* 2005;12:882–893.
21. Bolstad BM, Irizarry RA, Astrand M, Speed TP. A comparison of normalization methods for high density oligonucleotide array data based on variance and bias. *Bioinformatics.* 2003;19:185–193.
22. Zhu X, Craft CM. The carboxyl terminal domain of phosducin functions as a transcriptional activator. *Biochem Biophys Res Commun.* 2000;270:504–509.
23. van de Pavert SA, Meuleman J, Malysheva A, et al. A single amino acid substitution (Cys249Trp) in Crb1 causes retinal degeneration and deregulates expression of pituitary tumor transforming gene Pttg1. *J Neurosci.* 2007;27:564–573.
24. Fernandez-Medarde A, Barhoum R, Riquelme R, et al. RasGRF1 disruption causes retinal photoreception defects and associated transcriptomic alterations. *J Neurochem.* 2009;110:641–652.
25. Jiang G, Ke Y, Sun D, et al. A new model of experimental autoimmune keratoconjunctivitis sicca (KCS) induced in Lewis rat by the

autoantigen Klk1b22. *Invest Ophthalmol Vis Sci.* 2009;50:2245–2254.

26. Lu L, Wang S, Zheng L, et al. Amyotrophic lateral sclerosis-linked mutant SOD1 sequesters Hu antigen R (HuR) and TIA-1-related protein (TIAR): implications for impaired post-transcriptional regulation of vascular endothelial growth factor. *J Biol Chem.* 2009; 284:33989–33998.
27. Verpy E, Leibovici M, Zwaenepoel I, et al. A defect in harmonin, a PDZ domain-containing protein expressed in the inner ear sensory hair cells, underlies Usher syndrome type 1C. *Nat Genet.* 2000;26:51–55.
28. Williams DS, Aleman TS, Lillo C, et al. Harmonin in the murine retina and the retinal phenotypes of Ush1c-mutant mice and human USH1C. *Invest Ophthalmol Vis Sci.* 2009;50:3881–3889.
29. Samardzija M, Wenzel A, Aufenberg S, Thiersch M, Reme C, Grimm C. Differential role of Jak-STAT signaling in retinal degenerations. *FASEB J.* 2006;20:2411–2413.
30. Gariano RF, Gardner TW. Retinal angiogenesis in development and disease. *Nature.* 2005;438:960–966.
31. Mohand-Said S, Deudon-Combe A, Hicks D, et al. Normal retina releases a diffusible factor stimulating cone survival in the retinal degeneration mouse. *Proc Natl Acad Sci U S A.* 1998;95:8357–8362.
32. Campochiaro PA. Retinal and choroidal neovascularization. *J Cell Physiol.* 2000;184:301–310.
33. Green WR, Enger C. Age-related macular degeneration histopathologic studies: the 1992 Lorenz E. Zimmerman Lecture. *Ophthalmology.* 1993;100:1519–1535.
34. Liu L, Zhang R, Liu K, et al. Tissue kallikrein protects cortical neurons against in vitro ischemia-acidosis/reperfusion-induced injury through the ERK1/2 pathway. *Exp Neurol.* 2009;219:453–465.
35. Wu TH, Ting TD, Okajima TI, et al. Opsin localization and rhodopsin photochemistry in a transgenic mouse model of retinitis pigmentosa. *Neuroscience.* 1998;87:709–717.
36. Ueki Y, Wang J, Chollangi S, et al. STAT3 activation in photoreceptors by leukemia inhibitory factor is associated with protection from light damage. *J Neurochem.* 2008;105:784–796.
37. Penela P, Murga C, Ribas C, et al. G protein-coupled receptor kinase 2 (GRK2) in migration and inflammation. *Arch Physiol Biochem.* 2008;114:195–200.
38. Vroon A, Heijnen CJ, Kavelaars A. GRKs and arrestins: regulators of migration and inflammation. *J Leukoc Biol.* 2006;80:1214–1221.